Enhancing epicardial EMT to repair the heart

Dronkers, E.

4

Small molecule screen identifies novel activators of epithelial to mesenchymal transition in human epicardial cells

Esther Dronkers[1], Tessa van Herwaarden[1], Esmee J Groeneveld[1], Jesper Hjortnaes[2], Marie Jose Goumans[1], Anke M Smits[1]

[1] Department of Cell and Chemical Biology, Leiden University Medical Center, Leiden, The Netherlands.

[2] Department of Cardiothoracic Surgery, Leiden University Medical Center, Leiden, The Netherlands.

ABSTRACT

Since the adult heart has minimal capacity to repair itself, myocardial infarction often leads to pathological remodeling and ultimately to the development of fatal heart failure. Upon ischemic injury, the epicardium, the outer layer of the heart which is essential for cardiac development, becomes re-activated and displays reparative potential. In this process, epicardial epithelial-to-mesenchymal transition (epiMT) is an essential step. We hypothesize that the reparative capacity of the heart can be improved by enhancing the participation of the epicardium to cardiac repair, particularly by stimulating the occurrence of epiMT. Therefore the aim of this study is to identify novel epiMT-inducing compounds by performing a small molecule screen.

Primary epicardial cells were derived from human heart auricles and cultured as epithelial-like cells with a cobblestone morphology. Using these cells, a phenotypic screen was performed utilizing the LOPAC1280 small molecule library to identify epiMT-inducing compounds. EpiMT was defined using αSMA positive immunostaining as a hallmark for a phenotypic switch to a mesenchymal cell. After validation of the positive hits, five compounds were selected that reproducibly induced epiMT, as shown by: 1) a phenotypic switch towards mesenchymal spindle-shaped cells, 2) a decrease in CHD1 and 3) an increase in mesenchymal markers, such as Periostin. The selected compounds displayed low or absent toxicity to cultured cardiomyocytes and fibroblasts, indicating that the compounds can safely be applied to the heart. To identify a potential mechanism of epiMT induction, cells were treated for 3 hours with the two most promising compounds: TBBz and Oltipraz Metabolite M2 (M2), and subjected to RNA sequencing. This approach revealed that TBBz induced histone modifications and that M2 increased the transcription factor FOXQ1.

In conclusion, high-throughput experiments using human primary epicardial derived cells to identify novel epiMT-inducing compounds is feasible. Using this model, we have identified TBBz and Oltipraz Metabolite M2 as novel inducers of epiMT.

Keywords

Epicardium, EPDC, Primary Cell Culture, Cardiac Regeneration, Epithelial to Mesenchymal Transition, EMT, Small Molecule Screen

INTRODUCTION

After a myocardial infarction, the injured heart lacks the potential to repair itself resulting in the generation of a fibrotic scar. Because of this, cardiac function decreases causing the remaining viable tissue to be subjected to pathological remodeling. This compensatory remodeling ultimately progresses into heart failure. To date, no therapy is available to restore injured cardiac tissue. Identifying therapeutic targets to improve vascularization and cardiomyocyte proliferation after infarction are therefore ultimate goals in the field of cardiac research.

The epicardium, a mesothelial layer covering the entire surface of the heart, plays a vital role during development of the heart by providing cells and biochemical factors to the growing cardiac tissue (reviewed in (1)). By doing so, the epicardium contributes to key developmental processes, such as vascularization and myocardial compaction (2). These features of the epicardium are reactivated in the injured hearts of lower vertebrates, such as the zebrafish (3). Here, epicardial re-activation is essential for fully restoring lost cardiac tissue (4). Also in mammals, the recapitulation of embryonic epicardial processes aids in the repair process in the injured heart (5). Moreover, research has shown that the epicardial contribution to repair can be improved, e.g. by stimulating the epicardium with Thymosin β4 (6). Given the potential of epicardial cells in the context of the developing heart and in regenerative species, the epicardium emerges as an appealing target to enhance cardiac repair.

To partake in cardiac tissue generation, epicardial cells undergo epithelial to mesenchymal transition (epiMT) (7). In this process, epicardial cells lose their epithelial phenotype and delaminate from the epicardium to transform into motile mesenchymal cells. Typically, cells lose their epithelial proteins, such as E-cadherin (8), and gain mesenchymal markers, such as αSMA (9,10). These mesenchymal epicardial derived cells differentiate into fibroblasts, smooth muscle cells and pericytes (1) and secrete factors that promote vessel maturation (11) and cardiomyocyte proliferation (12,13). Trajectory analysis of the epicardium using RNA single cell sequencing suggested that epiMT occurs prior to fate specification (Mantri et al. and Lupu et al.), indicating that epiMT is an essential first step for the epicardial contribution to tissue formation and therefor a potential therapeutic target for the injured heart.

Given the importance of epiMT in epicardial behavior, the aim of this study is to identify novel inducers of epiMT. We exploited our previously developed cell culture model of human primary epicardial cells where epiMT can be induced in a controlled

fashion, (14) and subjected it to an array of pharmacologically active compounds. Our goal was to identify molecules that robustly induce epiMT on a phenotypic and molecular level. For future application in vivo, these factors should not be toxic to other cardiac cell types including cardiomyocytes, nor induce excessive proliferation of fibroblasts. Here, we demonstrate that a phenotypic high-throughput screen using primary human epicardial cells is feasible and effective. Using this screen, we identified two novel epiMT inducing compounds: TBBz and Oltipraz Metabolite M2. In addition, we may have identified alternative routes of epiMT induction.

MATERIAL AND METHODS

Cell culture

Human primary epicardial cells were isolated and cultured as described (15). Briefly, the epicardium was peeled of human heart auricles which are considered surgical waste and obtained anonymously under general consent. The epicardium was processed into a single cell suspension and cultured on gelatin coated plates in epicardial cell medium consisting of Dulbecco's modified Eagle's medium (DMEM low-glucose, Gibco) and Medium 199 (M199, Gibco) mixed in a 1:1 ratio, supplemented with 10% fetal bovine serum (heat inactivated for 25 minutes at 56 °C, Biowest), 100 U/mL penicillin (Roth) and 100 mg/mL streptomycin (Roth). Cells were cultured in the presence of 10 μM SB431542 (SB, Tocris) at 37 °C in 5% CO_2. Experiments were performed in cell culture medium without SB.

Human cardiac fibroblasts were derived from fetal hearts which were collected anonymously with informed consent. Three cell lines, derived from three individual fetal hearts, were cultured in Dulbecco's modified Eagle's medium (DMEM high-glucose, Gibco), supplemented with 10% fetal bovine serum, 100 U/mL penicillin (Roth) and 100 mg/mL streptomycin (Roth).

Induced pluripotent stem cells derived cardiomyocytes (iPSC-CM) were a kind gift of Dr. Buikema. The iPSC-CM were differentiated and matured for 30 days as previously described (16).

This research was carried out according to the official guidelines of the Leiden University Medical Center and approved by the local Medical Ethics Committee. This research conforms to the Declaration of Helsinki.

LOPAC1280 small molecule screen

Confluent epicardial cells were seeded in a 1:1 ratio in 50 µl epicardial cell medium in 8x384 wells plates per screen and incubated at 37 °C in 5% CO_2. The next day, 1280 biologically active small molecules derived from the LOPAC1280 library (Sigma) were diluted in 50 µl epicardial cell medium and added to the cells in a final concentration of 5 (screen A) or 10 µM (screen B and C) in such a way that the dimethylsulfoxide (DMSO) concentration was 0.5%. All conditions were performed in duplicate. In every culture plate, the following controls were included: SB (10 µM), control epicardial cell medium, DMSO (0.5%), and TGFβ3 (1 ng/mL, R&D systems). After 5 days, cells were fixed in 4% PFA. The total procedure has been executed 3 times. For screen A, epicardial cells isolated from two patients were mixed, for screen B and C individual patient isolations were used.

After fixation, cells were stained with mouse anti-h-αSMA conjugated 488 antibody as described below. To increase the fluorescent signal, cells were incubated with a secondary antibody (Alexa Fluor Ms-488, Thermo Scientific). Automatic imaging was performed using BDPathway™ Bioimager (BD Biosciences) for screen A and EVOS FL Auto 2 Imaging System (Thermo Fisher Scientific) for screen B and C, taking 4 images per well (2x2 at the center of the well, 10x magnification). For every picture, the number of DAPI+ nuclei and αSMA surface area was quantified using Cell Profiler software. Data analysis was performed using R. Measurements containing a divergent (either exceptionally high or low) number of DAPI+ nuclei were excluded, as they represent failed imaging. αSMA surface area was normalized for the controls present in its own plate to reduce inter-plate variability, using the following formula: $(SMA_{Compound} - SMA_{DMSO.mean})/(SMA_{TGFb.mean}-SMA_{DMSO.mean})*100\%$. For every screen the top 30 hits were selected, based on the αSMA value and taking into account the values of both duplicates. In addition, compounds present in the top 50 of more than 1 screen were also selected. These hits were confirmed by eyeballing the images to correct for artefacts. Compounds of interest were further validated in two additional individual cell isolations in a 96 well format.

Cell stimulations

The following compounds were used to stimulate cells: Phenamil methanesulfonate (10 µM, dissolved in DMSO, Sigma, p203), 3-deazaadenosine (20 µM, dissolved in mq, Biovision, 2771), H-8 dihydrochlride (10 µM, dissolved in DMSO, Sigma, M9656), TBBz (5 µM, dissolved in DMSO, Sigma, T6951), Oltipraz metabolite M2 (10 µM, dissolved in DMSO, SML0777, Sigma), SB431542 (10 µM, dissolved in DMSO, Tocris), DMSO, TGFβ3 (1 ng/mL, 4mM HCL/0.1%BSA, R&D systems). For the induction of epiMT, cells

were stimulated followed by isolation of RNA and protein after 5 days. To determine expression of epiMT-related transcription factors, RNA was isolated after 1.5, 3 and 24 hours of stimulation. To determine H3k27me3 levels, cells were stimulated for 3 hours. To determine cellular toxicity, IPSC-CM and cardiac fibroblast were stimulated for 48 hours whereafter an MTT assay was performed.

Immunocytochemistry

Cells were fixed in 4% PFA for 20 minutes at 4 °C followed by incubation with 1%BSA/PBS/Tw blocking buffer and overnight incubation with mouse anti-h-αSMA conjugated 488 antibody (R&D Ic1420g, 1:100), Vimentin (1:1000. ab195877, Abcam), Collagen 1 (1:200, 1310, Southern Biotech), Fibronectin (1:100, ab198933, Abcam), Phalloidin (1:1000, R415, Life Technologies) or Casein Kinase 2 alpha (MAB7957, 1 µg/mL, R&D systems). After washing, cells were incubated with the corresponding secondary antibodies (Alexa Fluor 488, 555 or 647, Thermo Scientific) and nuclei were stained using DAPI (Thermo Scientific). Imaging was conducted using the Leica AF6000.

qPCR

To determine gene expression profiles, RNA was isolated using ReliaPrep™ RNA Miniprep Systems (Promega). Concentration and purity of the RNA were determined using NanoDrop 1000 Spectrophotometer (Thermo Fisher Scientific). Next, cDNA synthesis was performed using the RevertAid H Minus First Strand cDNA Synthesis Kit (Thermo Fisher Scientific). Quantitative real time PCR was performed using SYBR Green (Promega) and run in 384 wells plates in technical triplicates on a CFX384 Touch™ Real-Time PCR Detection System (Bio-Rad). For every experiment and every primer set, mq and a cDNA sample without reverse transcriptase was taken along as negative controls. Expression levels were corrected for primer efficiency (Hellemans (2007)) determined by serial dilutions of three independent samples. For normalization, two reference genes (HPRT1 and TBP) were designed based on stable and robust expression in both epithelial and mesenchymal epicardial cells using geNORM (vandesompele 2002). Statistics were performed on the log transformed values.

Table 1 Primer sequences for qPCR

	Forward	Reverse
CDH1	CCC GGT ATC TTC CCC GC	CAG CCG CTT TCA GAT TTT CAT
CDH2	CAGACCGACCCAAACAGCAAC	GCAGCAACAGTAAGGACAAACATC
POSTN	GGAGGCAAACAGCTCAGAGT	GGCTGAGGAAGGTGCTAAAG
ACTA2	CCGGGAGAAAATGACTCAAA	GAAGGAATAGCCACGCTCAG
NR1H3	ATCCCCATGACCGACTGATG	CTCCCAGGAATGTTTGCCCT
SNAI1	CCAGTGCCTCGACCACTATG	CTGCTGGAAGGTAAACTCTGGA
SNAI2	CGGACCCACACATTACCTTGT	TTCTCCCCCGTGTGAGTTCTA
HPRT1	CTCATGGACTGATTATGGACAGGAC	GCAGGTCAGCAAAGAACTTATAGCC
TBP	TGGAAAAGTTGTATTAACAGGTGCT	GCAAGGGTACATGAGAGCCA

MTT assay

Fibroblasts were seeded in 96 wells and stimulated with indicated compounds for 48 hours after which DMEM containing MTT (0.5 mg/mL, Sigma) was added for 3 hours. Solubilization was performed by adding DMSO to the well whereafter absorbance was measured at 595 nm.

TUNEL staining

IPSC-CM were stimulated for 48 hours and fixed in 4% PFA. Cells were permeabilized in 0.25% TX100/PBS for 15 minutes and subsequently blocked in 1% BSA/PBS. TUNEL solution (ratio enzyme and label solution 1:25) was applied for 60 minutes. Next, cells were washed, blocked in 2% BSA/0.1% TX100/PBS/ and incubated for 2 hours with goat anti-cTnI (Hytest, 4T21, 1:200) antibody followed by one hour incubation with secondary antibody (Alexa Fluor 488, Thermo Scientific). DAPI was used as counter-staining (Thermo Scientific). Imaging was executed by EVOS FL Auto 2 Imaging System (Thermo Fisher Scientific).

Western Blot

Cells were lysed in radio immunoprecipitation assay (RIPA) buffer supplemented with protease inhibitors (Complete protease inhibitor cocktail tablets, Roche Diagnostics) and phosphatase inhibitors (1M NaF, 10% NaPi, 0.1M NaVan). Protein concentration was determined using a BCA assay (Pierce BCA Protein Assay Kit, 23225, Thermo Scientific). Samples were diluted to equal concentrations and loaded onto a 10% SDS-polyacrylamide gel followed by transfer to an Immobilon-P transfer membrane (# IPVH00010, PVDF membrane, Millipore) at 4°C. Blots were blocked in 5%BSA/TBST for 30 minutes at room temperature. Immunodetection was performed by over-night incubation at 4 °C with anti-E-cadherin (1:5000, ab40772, Abcam), anti-SMA

(1:500, A2547, Sigma-Aldrich), anti-Vinculin (1:5000, V9131, Sigma-Aldrich), anti-Phospho-CK2-Substrate Rabbit mAb mix (1:1000, #8738, Cell Signaling), anti-H3K27me3 (1:2500, 17622, Millipore) and subsequent incubation with Sheep anti-mouse HRP (NA931, GE Healthcare) or donkey anti-Rabbit HRP (ab98493, Abcam) for 30 minutes at room temperature, followed by chemiluminescent imaging using WesternBright ECL HRP substrate. Blots were imaged using ChemiDoc (Bio-rad).

RNA sequencing

Epicardial cells isolated from three patients (n=3) were incubated for 3 hours in epicardial cell medium supplemented with 0.1% DMSO, TGFβ3 (1 ng/mL, R&D systems) plus DMSO, TBBz (5 μM), or M2 (10 μM). Total RNA was isolated as described above; and quality and integrity were assessed using an Agilent bioanalyzer. Library preparation, mRNA sequencing and data analysis was executed by Novogene Co., Ltd using the Illumina platform with a sequencing depth of 15G per sample. Reads containing adapters, reads with N > 10%, and low-quality reads were removed. The Q20, Q30 and GC content were established for quality control. The clean reads were mapped against the human reference genome (ensembl_homo_sapiens_grch38_p12_gca_000001405_27) using STAR software. Gene expression levels were estimated as expected number of Fragments Per Kilobase of transcript sequence per Millions base pairs sequenced (FPKM). Clustering was determined using the log2(FPKM+1) value and differentially expressed genes (DEGs) were calculated using the DESeq2 R-package. Genes with an adjusted p-value <0.05 were considered as DEGs.

Statistics

For every experiment, the n number is denoted in the legend, indicating biological repeats: the number of individual cell isolations that have been used. Displayed pictures are representative for multiple observations. Statistics were performed using Graphpad Prism 9 software. For every experiment, the performed statistical test is indicated in the figure legend. Only relevant comparisons were statistically tested. Significance was considered when $P<0.05$.

RESULTS

Human primary epicardial cells were isolated from human heart auricles. The epicardial cells were expanded in the presence of ALK4/5/7 kinase inhibitor SB431542 (SB) to maintain their epithelial phenotype which was evident by their cobblestone morphology. EpiMT was induced by TGFβ stimulation, which elicited a drastic phenotypical

transformation towards spindle-shaped cells, as previously described (14). To identify novel inducers of epiMT, we established an in vitro model for a high throughput phenotypical assay. First, we selected a proper and robust read out for epiMT by testing multiple antibodies for immunofluorescent analysis. The monoclonal mouse IgG2a clone #1A4 against human αSMA from R&D (IC1420G) conveyed the highest discrimination between untreated cobblestone and spindle-shaped cells and was therefore selected for the screen read-out (Fig. S1). To screen for epiMT inducers, cobblestone epicardial cells were seeded in 384-wells plates and were incubated with small molecules derived from the Library of Pharmacologically Active Compounds (LOPAC1280). This library consists of small molecules dissolved in DMSO targeting a wide range of cell signaling processes. For every cell culture plate, DMSO-treated cells were included as a negative control, and TGFβ-treated cells as a positive control. Furthermore, SB treated cells and untreated cells were taken along as additional controls for the αSMA staining (Fig. 1A).

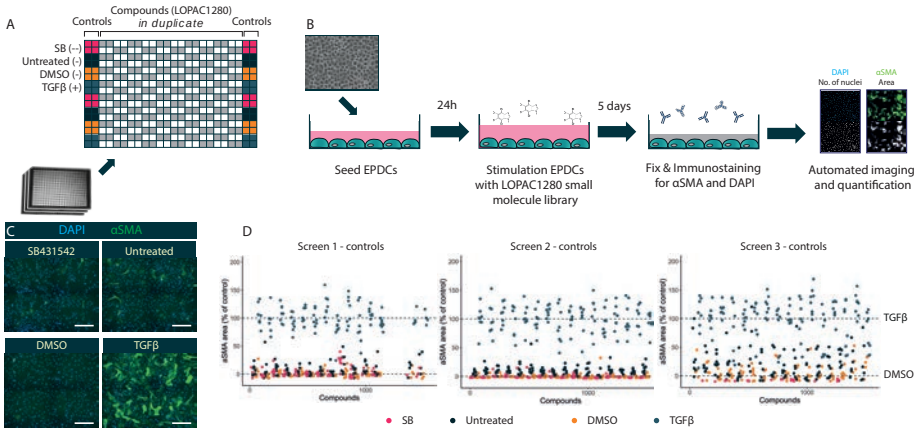

Figure 1 | **Design of phenotypic LOPAC1280 compound screen.** (A) Plate design of phenotypic LOPAC1280 compound screen. Eight 384 wells plates were used, each plate included control conditions SB, Untreated, DMSO and TGFβ. Compounds were added in duplicate. (B) Design of experiment. Cobblestone human primary epicardial derived cells were seeded and after 24 hours stimulated with compounds derived from the LOPAC1280 library. After 5 days of stimulation, cells were fixed and stained for αSMA and DAPI which were subsequently automatically imaged and quantified. (C) Representative images of controls. Scale bar: 50 μm. (D) Quantification of control conditions of the three individual screens displayed as αSMA area relative to DMSO and TGFβ treated cells. The X-axis shows the number of the condition (first plate is 1-192, second plate is 193-384, etc). Every dot represents one well.

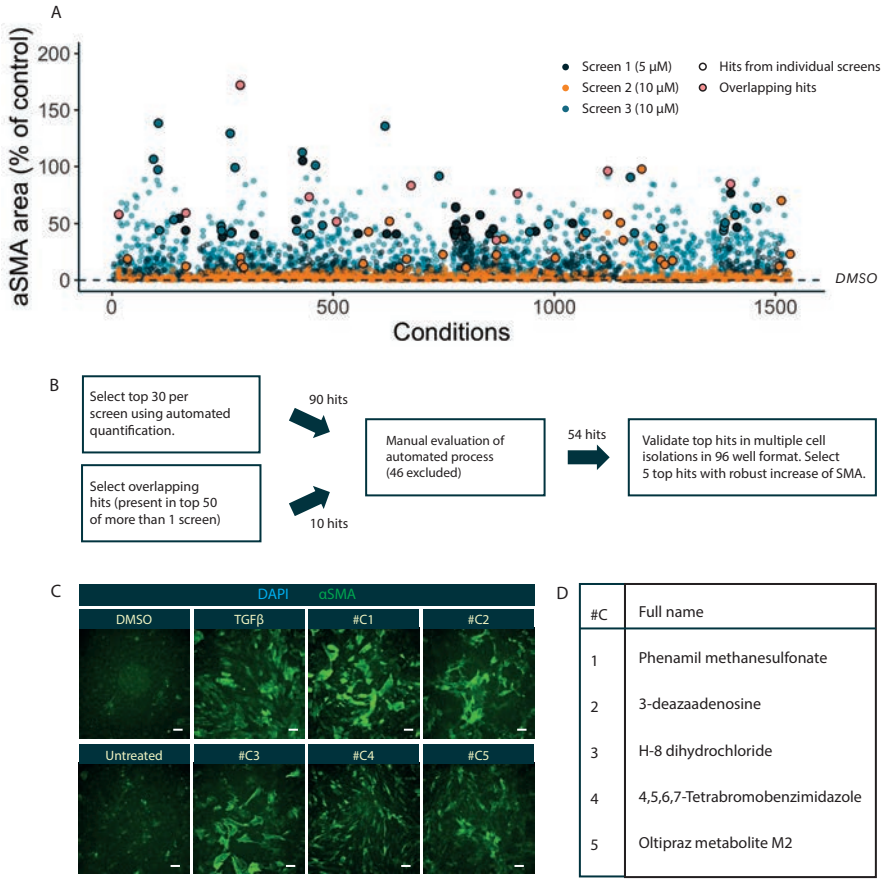

Figure 2 | Phenotypic compound screen identifies five potential epiMT inducers. (A) Results of the compound screen displayed as aSMA area relative to DMSO and TGFβ treated cells. The X-axis shows the number of the condition (first plate is 1-192, second plate is 193-384, etc). Every dot represents one well. (B) Schematic overview of the selection process leading to the final five hits. (C) Immunofluorescent staining of aSMA and DAPI of the five identified compounds and their controls after 5 days of stimulation (n=2-3). Scale bar: 100 µm. (D) List of the five selected molecules.

All conditions were tested in duplicate. We performed the screen three times, in epicardial cells isolated from different patients to account for patient variability, and in two concentrations (5 µM and 10 µM). After 5 days of incubation, the cells were fixed and stained for αSMA (Fig. 1B, C). αSMA-staining was automatically imaged and quantified as total area of positive αSMA immunostaining normalized against positive staining in control cells. The controls of the three individual screens are depicted in Fig.1D. In the first screen, we encountered technical difficulties with one cell culture

plate which is displayed as a gap in the figure. Screen 3 shows higher variation within each control condition compared to screen 1 and 2, shown by the spread of the dots. As expected, the percentage αSMA area is lower in all three negative control conditions. Interestingly, DMSO treatment seemed to lower αSMA expression compared to untreated cells. Overall, there is a clear distinction between the negative controls and the positive control TGFβ, indicating that this set-up is effective to identify novel epiMT inducers.

The results of all three screens are combined in Fig. 2A, where every dot represents one well. To select compounds for further analysis, we started by evaluating the compounds that induced αSMA expression in more than one screen. Compounds that scored within the top 50 in more than one screen were listed (10 compounds, Fig. 2B and supplementary table 4). In addition, to ensure we did not miss any potential epiMT inducer, we also selected the top 30 hits from every screen (see supplementary table 1, 2 and 3). The pictures taken of these hits were evaluated manually and images containing artefacts were excluded, which resulted in a list of 54 compounds of interest. This selection was subjected to another round of testing in epicardial cells after which five small molecules were selected based on their capacity to robustly increase αSMA expression, and to elicit morphological changes towards spindle-shaped cells in cells isolated from multiple patients (Fig. 2C-D).

We continued with five selected compounds and validated their effect on epiMT in more detail. First, we optimized the working concentration for all five compounds, defined as the lowest concentration that elicited αSMA induction (data not shown). Next, we evaluated the morphology of the epicardial cells after compound stimulation. All small molecules induced a clear transition towards spindle-shaped mesenchymal cells compared to DMSO and untreated (Fig. 3A). Interestingly, there were morphological differences between the different stimulations, e.g. #C4' induced spindles displayed long dendritic-like tails while #C1' induced spindles have a thick and round body, with short tapered protrusions (Fig. 3A). Such variations were also observed in the αSMA immunostaining pattern (Fig. 2C), e.g. #C3' induced spindles demonstrated a smooth muscle cell like striated pattern in large dissimilar cells, while #C5' induced spindles displayed a gradient of staining intensity and smaller, more rectangular-shaped cells. The variety in morphology between the compounds indicates that the five small molecules may not induce mesenchymal differentiation via the same mechanism or pathway. To confirm the morphological observed epiMT, gene profiling was performed to establish regulation of epiMT related genes. For all small molecules, the expression of CDH1 (encoding E-cadherin) decreased massively (Fig. 3B), demonstrating the loss

of epithelial morphology. This was corroborated by the loss of E-cadherin protein (Fig. 3D). Furthermore, almost all molecules, except for #C2, showed a trend towards an increase of CDH2 (encoding N-cadherin), which is a hallmark of a mesenchymal phenotype. For #C1, #C2 and #C3, the transition of E-cadherin to N-cadherin was not apparent in all tested epicardial cell isolations, which can be appreciated from the spread of the individual dots, suggesting that epiMT induction is less robust. We continued by determining the presence of the mesenchymal marker Periostin (POSTN) which was 10-fold increased in almost all stimulations (Fig. 3C).

Although we could not detect massive changes in ACTA2 gene regulation (Fig. 3C), αSMA protein levels were upregulated in cell cultures stimulated with #C3, #C4 and #C5 (Fig. 3D). To conclude, while not to the same extend, the identified five small molecules all induce epiMT both phenotypically, and at a molecular and protein level.

For compounds to be used for in vivo stimulation of the epicardium, it is essential that they do not harm other cardiac cell types at concentrations required for the induction of epiMT. Therefore, we determined the toxicity of the compounds in cardiomyocytes and fibroblasts. Toxicity of the compounds in iPSC-CM (Fig. 4A) was determined by TUNEL staining and cell numbers, which was quantified by counting DAPI+ nuclei. Only at very high concentrations (>4x the working concentration), a small effect on cell death was observed for #C1 and #C4 (Fig. 4B). Furthermore, the identified small molecules did not induce the proliferation of cardiac fibroblasts, nor did they exert any harmful effects on these cells when stimulated with the working concentration, although 4x the working concentration of #C1 and #C4 was toxic for the cells, while #C2 was able to induce slight fibroblast proliferation (Fig. 4C). To conclude, at the working concentration, all compounds appear safe for cardiomyocytes and fibroblasts.

Based on their ability to induce epiMT and their robustness in doing so, we decided to continue with the two most promising compounds namely 4,5,6,7-Tetrabromobenzimidazole (TBBz, #C4) and Oltipraz metabolite M2 (M2, #C5), and studied the underlying mechanism of their epiMT induction. An essential step in the process of epiMT is the upregulation of EMT regulating transcription factors. In our epicardial cell culture model, TGFβ mainly induces epiMT via the upregulation of SNAI1 (encoding SNAIL)(Fig. 5A). Interestingly, TBBz and M2 mainly induced the expression of SNAI2 (encoding SLUG) (Fig. 5A) suggesting that both compounds follow a different pathway than TGFβ to induce epiMT. Noteworthy, M2 induced SNAI2 within 90 minutes, while upon TBBz stimulation this transcription factor is mainly upregulated after 24 hours, suggesting an indirect epiMT-induction.

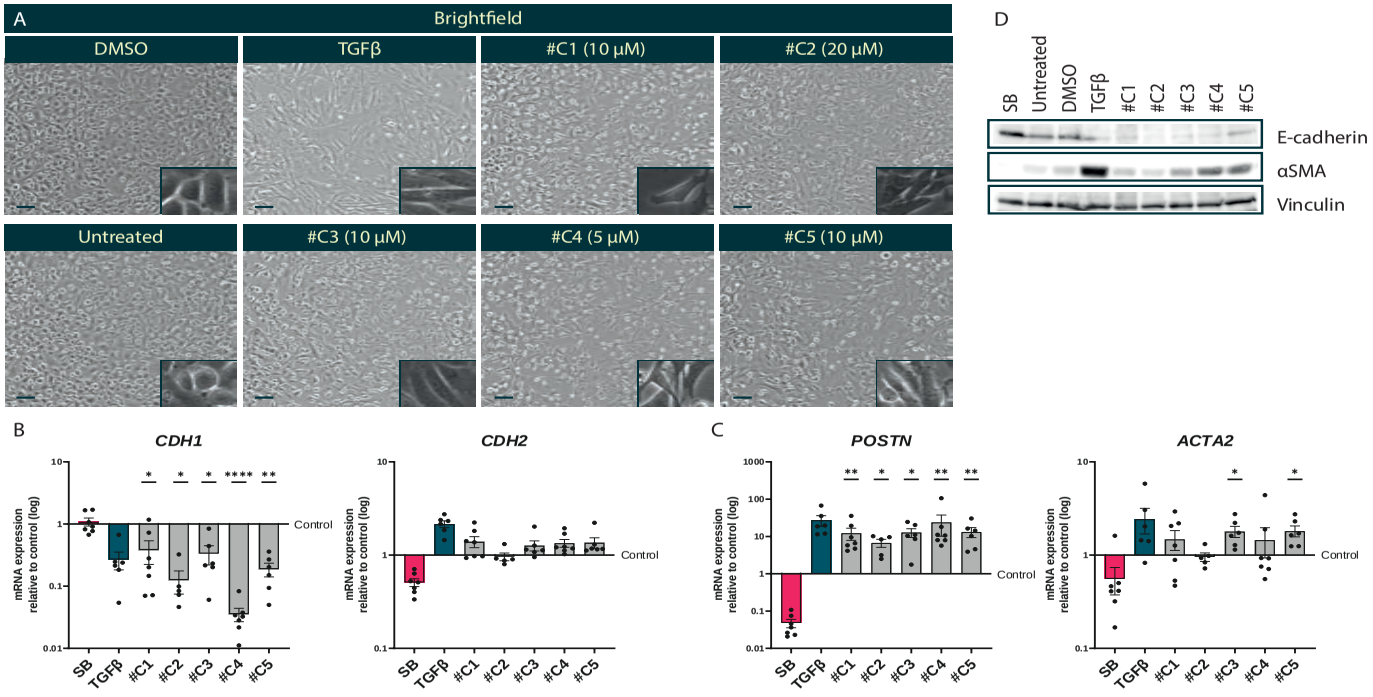

Figure 3 | Identified hits induce epiMT on molecular and protein level

(A) Representative brightfield images of the five identified hits and their control conditions (n=7). Working concentration of each compound is displayed in the title. Scale bar: 100 µm. (B) mRNA expression levels for CDH1 and CDH2 relative to control (DMSO or mQ) determined in the five identified compounds after 5 days of stimulation (n=7, mixed-effects analysis, Sidak's multiple comparisons test, * = $p < 0.05$, ** = $p < 0.01$, ** = $p < 0.001$, ** = $p < 0.0001$) (C) Representative western blot of protein expression levels for E-cadherin, αSMA and loading control Vinculin for the five identified compounds (n=3).

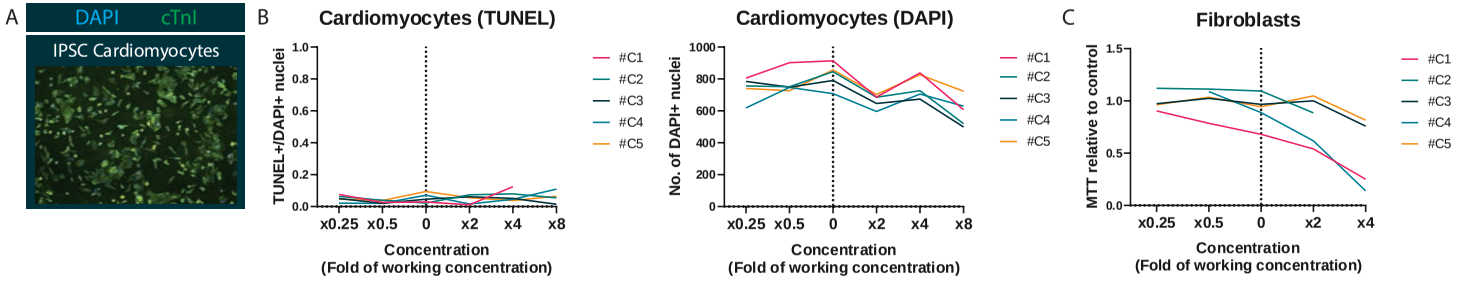

Figure 4 | Identified compounds do not harm cardiomyocytes and fibroblasts in vitro

(A) Representative picture of immunofluorescent staining for cTnI and DAPI of induced pluripotent stem cell (IPSC) derived cardiomyocytes. (B) Quantification of TUNEL staining of IPSCs-CMs exposed to increasing concentrations of the five identified compounds, displayed as the number of TUNEL+ nuclei divided by the number of DAPI+ nuclei (n=1). The number of DAPI+ nuclei are also separately displayed. Concentration is shown as fold of the working concentration. (C) Quantification of MTT assay on fetal cardiac fibroblasts exposed to increasing concentrations of the five identified compounds, displayed relative to their control (DMSO or mQ treated cells) (n=3). Concentration is displayed as fold of the working concentration.

To understand the underlying mechanism of epiMT induction, we focused on the known function of the identified compounds. TBBz is mostly described as an inhibitor of casein kinase 2 (CK2), which is present in many cell types including epicardial cells (Fig. S2) and has been related to EMT via FOXC2 (17). Interestingly, using an antibody against phosphorylated CK2 substrate, we did not observe an effect of TBBz on CK2 activity in epicardial cells (Fig. S2). The LOPAC1280 library includes a highly similar CK2 inhibitor, TBB, which did not induce αSMA expression in any of our screens. Furthermore, another CK2 inhibitor, CX4945 did not induce epiMT to the same extend as TBBz. Altogether, our data indicates that TBBz elicits epiMT in a CK2 independent manner (Fig. S2).

M2 has been implicated in several processes, including liver X receptor α (LXRα) transcriptional activity, which has been associated with EMT (18). However, no effect of M2 on mRNA expression of LXRα was found in epicardial cells after 5 days of stimulation (Fig. S3).

In search of a epiMT inducing mechanism, we used an unbiased approach to investigate the direct effect of TBBz and M2 on three independent epicardial cell isolations by stimulating the cells for 3 hours and profiling all cell signaling processes using RNA sequencing (Fig. 5B). As controls, DMSO and TGFβ treated cells were included. The heatmap in Fig. 5C shows that both TGFβ and TBBz induce a strong and distinct response, displayed by a large number of differentially expressed genes compared to the DMSO treated samples and between these two conditions. TBBz induces a large set of DEGs (Fig. 5D), which are mainly involved in histone modification and histone lysine methylation (Fig. 5G). Zooming in on the specific genes that are involved in this reveals that genes encoding methyltransferases are downregulated by TBBz.

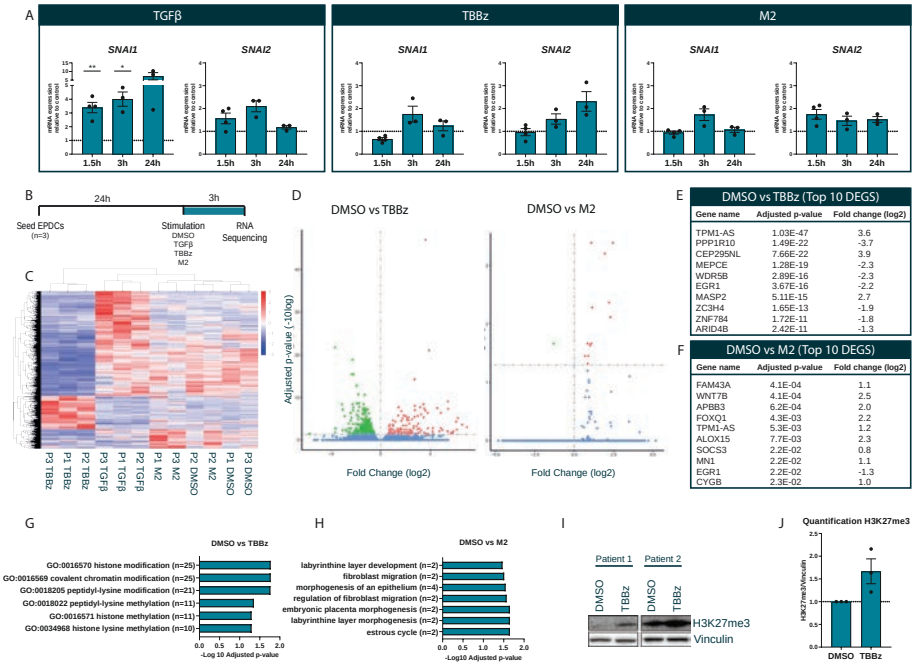

Figure 5 | RNA sequencing reveals direct targets of TBBz and M2 in epicardial cells

(A) mRNA expression levels for SNAI1 and SNAI2 in epicardial cells stimulated for 1.5, 3 or 24 hours with TGFβ, TBBz or M2 relative to control (n=3-4, mixed-effects analysis, Sidak's multiple comparisons test). (B) Schematic overview of experimental design. (C) Heatmap derived from RNA sequencing of three epicardial cell isolations (P1-P3) stimulated with DMSO, TGFβ+DMSO, TBBz or M2 for 3 hours. Samples and genes were clustered using the log2(FPKM+1) values. Red and blue indicate respectively high and low expression levels. (D) Volcano plot of differentially expressed genes (DEGs) of DMSO versus TBBz treated epicardial cells, and DMSO versus M2 stimulated epicardial cells. Green and red dots respectively indicate DEGs that are significantly downregulated or upregulated. (E) List of ten most significant DEGs of DMSO versus TBBz treated epicardial cells and their fold change difference. (F) List of ten most significant DEGs of DMSO versus M2 treated epicardial cells and their fold change difference. (G) Adjusted p-value of the significantly enriched GO terms in DMSO versus TBBz treated epicardial cells. Counts (n) indicate the number of differentially expressed genes concerning this GO term. (H) Adjusted p-value of the significantly enriched GO terms in DMSO versus M2 treated epicardial cells. Counts (n) indicate the number of differentially expressed genes concerning this GO term. (I) Representative western blot for protein expression levels of H3K27me3 and loading control Vinculin for epicardial cells derived from 2 patients treated with DMSO (n=3), TBBz (n=3) for 3 hours. (J) Quantification of the western blot in H for DMSO and TBBz conditions (n=3).

This suggests that TBBz may induce epiMT via epigenetic regulation. To further investigate this, we determined the effect of TBBz on H3K27 trimethylation (H3K27me3), a post-translational modification that has been related to EMT regulation (19). Although not significant, in three cell lines we observed an increase is H3k27me3 upon stimulation with TBBz (Fig. 5I and J). This was not observed by other epiMT-inducing stimulations, such as TGFβ (Fig. S4). In contrast to TBBz, M2 stimulations elicited only 14 DEGs (Fig. 5D). One gene that seemed particularly interesting in this setting was the upregulation of FOXQ1 (Fig. 5F), a known regulator of EMT but yet undescribed in epiMT. In summary, TBBz and M2 induce epiMT in a different manner than TGFβ does as they do not induce the same EMT-TF, nor do they exhibit a similar genetic profile 3h after stimulation. TBBz induces a large shift in the epigenetic landscape by increasing H3K27me3 causing a delayed upregulation of SNAI2 and induction of epiMT. M2 likely induces epiMT via upregulation of FOXQ1 and SNAI2.

DISCUSSION

In this study, we developed a high throughput in vitro screening protocol using human primary epicardial cells and identified two novel inducers of epicardial epithelial to mesenchymal transition (epiMT).

To be able to perform a phenotypic screen, we exploited our previously described in vitro model in which human epicardial cells display a clear phenotypical switch between their epithelial and mesenchymal phenotype (14,15). The use of primary cells serves the benefit of representing the biological variability within the human epicardium and therefore is highly translational. This benefits over the difficulties that come with using human primary cells, such as the availability of cardiac tissue, and the challenge to achieve a sufficiently high number of cells to execute such a screen. As read-out, we selected a marker that provides a high contrast between the negative control (untreated) and the positive control (TGFβ). The mesenchymal marker αSMA turned out to be most distinctive, specifically the antibody offered by R&D (Ic1420g). αSMA is a marker for mesenchymal cells and more specifically for pericytes, myofibroblasts and smooth muscle cells. As with every antibody-based read-out, using αSMA likely biased our results and consequently we may have missed epiMT inducing compounds which did not induce αSMA. For example, basic fibroblast growth factor (BFGF) induces epiMT without the upregulation of αSMA (20) and would not be picked up by our screening. Our list is therefore not exhaustive but nevertheless provided sufficient hits. To conclude, we provided a relatively easy and effective

model to study epicardial behavior which may pave the way for basic research or drug discovery in epiMT, and other epicardial read-outs such as proliferation, differentiation, and toxicity.

Using automated imaging, quantification of αSMA expression, and subsequent validation, we initially selected five hits. Based on the description of these compounds provided by the LOPAC1280 library, we could not discover one common signaling pathway among these hits. In addition, the compound-induced mesenchymal cells displayed distinct morphologies. This suggest that the identified compounds do not directly or only indirectly activate the same pathway resulting in epiMT. Since epiMT is an intricate process, defined as plastic transition between two extremes with several intermediate stages (21), we found it essential to determine if the compounds induce full epiMT. Therefore, we used a variety of tests; we reported cell morphology, a decrease in epithelial markers and an increase in mesenchymal markers, both at the level of mRNA and protein and we show the presence of EMT transcription factors. This broad approach provided two reliable and robust epiMT inducers.

Research into epiMT has already established that TGFβ, Wnt and PDGF are its main regulators, mostly via WT1 but also other transcription factors such as TCF21 and SOX9 (reviewed in (22)). In our study, we identified two novel regulators. TBBz is a CK2 inhibitor and off target effects are barely described for this molecule. However, in our hands, we could not find an effect of TBBz on CK2 activity, and conversely other CK2 inhibitors did not elicit the same epiMT induction as TBBz. Although it is possible that this is due to technical issues, we consider that TBBz does not act on epiMT via CK2. Interestingly, RNA sequencing revealed that TBBz signals via downregulation of histone methyltransferases. The fact that EMT-TF SLUG is upregulated after 24 hours suggests that the changes in the epigenetic landscape lead to the upregulation of SLUG and consequently the induction of epiMT. Epigenetic regulation of epiMT has been described before (23–25). In addition to this, it has been shown that injury induces major changes in chromatin accessibility of epicardial cells in zebrafish which also points to a significant role for epigenetic regulation in injury-induced epicardial behavior (26). Interestingly, increased levels of KDM6A were shown to prevent epiMT in vitro by repressing H3K27Me3(24). This is in line with our data, showing that TBBz increases levels of H3K27Me3 and induces epiMT. Furthermore, protein arginine methyltransferase 1 (PRMT1) was shown to induce epiMT in the developing heart, most likely via SLUG (25). This demonstrates that histone modification, especially methyltransferases, are of relevance in epiMT regulation and can be exploited to target epiMT. For this, TBBz is a good starting point.

Oltipraz Metabolite M2 induces only a few genes and therefore seems to hit a more specific target. Within 1.5 hours, SLUG is upregulated and maintained over at least 24 hours. One of the differentially expressed genes in the first 3 hours is FOXQ1, a transcription factor that has been related to EMT (27) but not to the epicardium. Further experiments are required to determine which role FOXQ1 plays in M2-induced epiMT.

To conclude, it is feasible and effective to conduct a phenotypic high throughput compound screen using primary epicardial cells. Using this approach, we have identified two novel inducers of epiMT: TBBz, that induces histone modifications, and Oltipraz Metabolite M2 which increases FOXQ1.

ACKNOWLEDGEMENT

We thank Lucia Clemens-Daxinger and Maja Vukic for their help with the H3K27me3 western blot.

REFERENCES

1. Smits AM, Dronkers E, Goumans M-JJ. The epicardium as a source of multipotent adult cardiac progenitor cells: Their origin, role and fate. Pharmacol Res. 2018 Jan 24;127:129–40.
2. Gittenberger-de Groot AC, Vrancken Peeters M-PFM, Bergwerff M, Mentink MMT, Poelmann RE. Epicardial Outgrowth Inhibition Leads to Compensatory Mesothelial Outflow Tract Collar and Abnormal Cardiac Septation and Coronary Formation. Circ Res. 2000 Nov 24;87(11):969–71.
3. Lepilina A, Coon AN, Kikuchi K, Holdway JE, Roberts RW, Burns CG, et al. A Dynamic Epicardial Injury Response Supports Progenitor Cell Activity during Zebrafish Heart Regeneration. Cell. 2006;127(3):607–19.
4. Wang J, Cao J, Dickson AL, Poss KD. Epicardial regeneration is guided by cardiac outflow tract and Hedgehog signalling. Nature. 2015 Jun 4;522(7555):226–30.
5. Duan J, Gherghe C, Liu D, Hamlett E, Srikantha L, Rodgers L, et al. Wnt1/βcatenin injury response activates the epicardium and cardiac fibroblasts to promote cardiac repair. EMBO J. 2012 Jan 18;31(2):429–42.
6. Smart N, Bollini S, Dubé KN, Vieira JM, Zhou B, Davidson S, et al. De novo cardiomyocytes from within the activated adult heart after injury. Nature. 2011;474(7353):640–4.
7. Pérez-Pomares JM, Macías D, García-Garrido L, Muñoz-Chápuli R. Contribution of the primitive epicardium to the subepicardial mesenchyme in hamster and chick embryos. Dev Dyn. 1997 Oct;210(2):96–105.
8. Martínez-Estrada OM, Lettice LA, Essafi A, Guadix JA, Slight J, Velecela V, et al. Wt1 is required for cardiovascular progenitor cell formation through transcriptional control of Snail and E-cadherin. Nat Genet. 2010 Jan 20;42(1):89–93.
9. Cano E, Carmona R, Ruiz-Villalba A, Rojas A, Chau Y-Y, Wagner KD, et al. Extracardiac septum transversum/proepicardial endothelial cells pattern embryonic coronary arterio–venous connections. Proc Natl Acad Sci. 2016 Jan 19;113(3):656–61.
10. Liu Q, Zhang H, Tian X, He L, Huang X, Tan Z, et al. Smooth muscle origin of postnatal 2nd CVP is pre-determined in early embryo. Biochem Biophys Res Commun. 2016 Mar;471(4):430–6.
11. Quijada P, Trembley MA, Misra A, Myers JA, Baker CD, Pérez-Hernández M, et al. Coordination of endothelial cell positioning and fate specification by the epicardium. Nat Commun. 2021 Dec 6;12(1):4155.
12. Lavine KJ, Yu K, White AC, Zhang X, Smith C, Partanen J, et al. Endocardial and epicardial derived FGF signals regulate myocardial proliferation and differentiation in vivo. Dev Cell. 2005 Jan;8(1):85–95.
13. de Bakker DEM, Bouwman M, Dronkers E, Simões FC, Riley PR, Goumans M-J, et al. Prrx1b restricts fibrosis and promotes Nrg1-dependent cardiomyocyte proliferation during zebrafish heart regeneration. Development. 2021 Oct 1;148(19).

14. Moerkamp AT, Lodder K, van Herwaarden T, Dronkers E, Dingenouts CKE, Tengström FC, et al. Human fetal and adult epicardial-derived cells: a novel model to study their activation. Stem Cell Res Ther. 2016 Dec 29;7(1):174. A

15. Dronkers E, Moerkamp AT, van Herwaarden T, Goumans M-J, Smits AM. The Isolation and Culture of Primary Epicardial Cells Derived from Human Adult and Fetal Heart Specimens. J Vis Exp. 2018 Apr 24;134:e57370.

16. Maas RGC, Lee S, Harakalova M, Snijders Blok CJB, Goodyer WR, Hjortnaes J, et al. Massive expansion and cryopreservation of functional human induced pluripotent stem cell-derived cardiomyocytes. STAR Protoc. 2021 Mar;2(1):100334.

17. Golden D, Cantley LG. Casein Kinase 2 prevents mesenchymal transformation by maintaining Foxc2 in the cytoplasm HHS Public Access. Oncogene. 2015;34(36):4702–12.

18. Ji L, Zhang B, Zhao G. Liver X receptor α (LXRα) promoted invasion and EMT of gastric cancer cells by regulation of NF-κB activity. Hum Cell. 2017 Apr 16;30(2):124–32.

19. Segelle A, Núñez-Álvarez Y, Oldfield AJ, Webb KM, Voigt P, Luco RF. Histone marks regulate the epithelial-to-mesenchymal transition via alternative splicing. Cell Rep. 2022 Feb;38(7):110357.

20. Witty AD, Mihic A, Tam RY, Fisher SA, Mikryukov A, Shoichet MS, et al. Generation of the epicardial lineage from human pluripotent stem cells. Nat Biotechnol. 2014 Oct 21;32(10):1026–35.

21. Nieto MA, Huang RY-J, Jackson RA, Thiery JP. Emt: 2016. Cell. 2016;166(1):21–45.

22. Quijada P, Trembley MA, Small EM. The Role of the Epicardium During Heart Development and Repair. Circ Res. 2020 Jan;126(3):377–94.

23. Vieira JM, Howard S, Villa del Campo C, Bollini S, Dubé KN, Masters M, et al. BRG1-SWI/SNF-dependent regulation of the Wt1 transcriptional landscape mediates epicardial activity during heart development and disease. Nat Commun. 2017 Dec 24;8(1):16034.

24. Qureshi R, Kindo M, Boulberdaa M, von Hunolstein J-J, Steenman M, Nebigil CG. A prokineticin-driven epigenetic switch regulates human epicardial cell stemness and fate. Stem Cells. 2018 Jun 6;(Umr 7242).

25. Jackson-Weaver O, Ungvijanpunya N, Yuan Y, Qian J, Gou Y, Wu J, et al. PRMT1-p53 Pathway Controls Epicardial EMT and Invasion. Cell Rep. 2020 Jun 9;31(10).

26. Cao Y, Xia Y, Balowski JJ, Ou J, Song L, Safi A, et al. Identification of enhancer regulatory elements that direct epicardial gene expression during zebrafish heart regeneration. Development. 2022 Feb 15;149(4).

27. Qiao Y, Jiang X, Lee ST, Karuturi RKM, Hooi SC, Yu Q. FOXQ1 Regulates Epithelial-Mesenchymal Transition in Human Cancers. Cancer Res. 2011 Apr 15;71(8):3076–86.

SUPPLEMENTARY FIGURES & TABLES

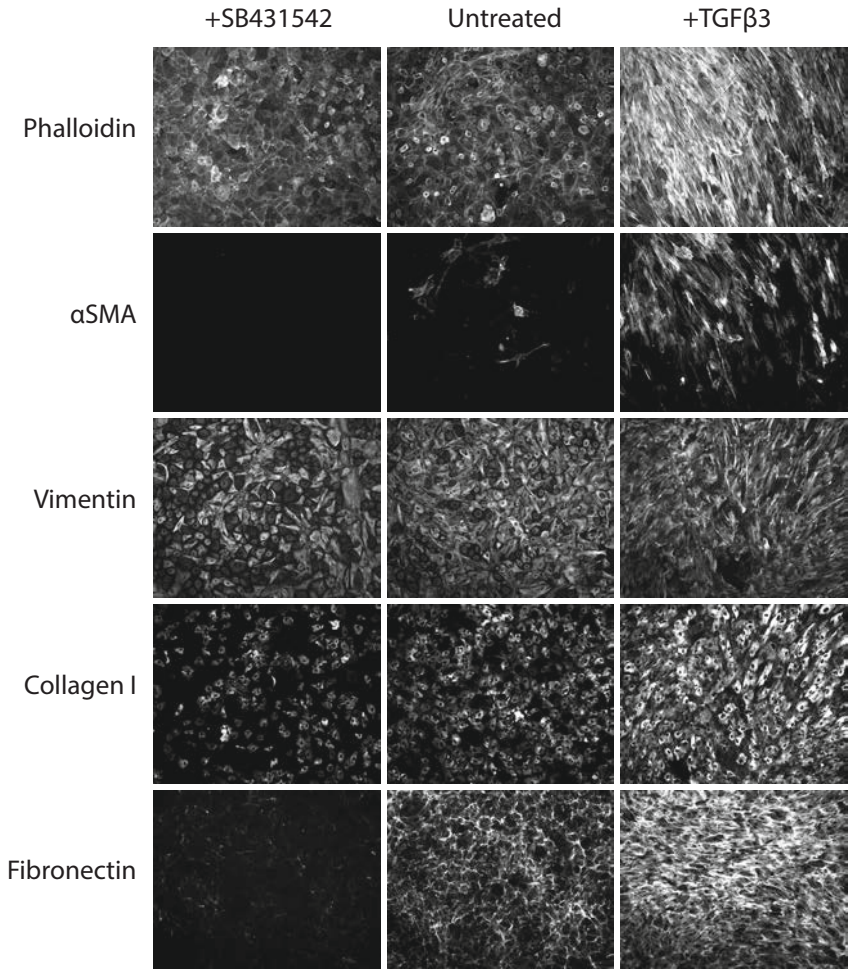

Fig. S1 | αSMA immunostaining can be used as a read out for epiMT
Representative immunostainings of epicardial cells that were treated with SB431542 (SB), TGFβ or with epicardial cell medium for 5 days.

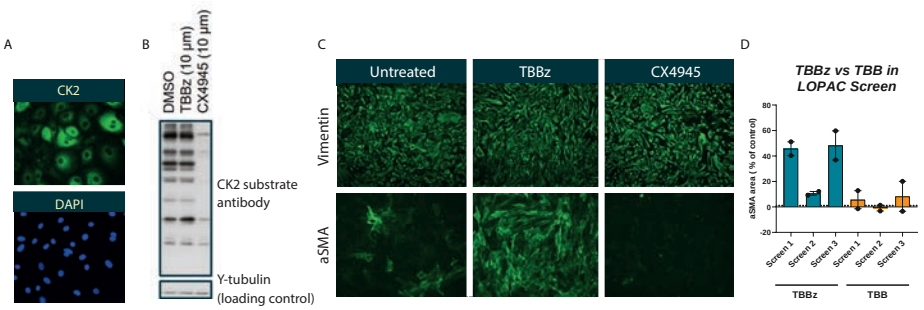

Fig S2 | TBBz may not induce epiMT via CK2

(A) Representative immunostaining for CK2α in epicardial cells. (B) Representative image of western blot of epicardial cells treated with DMSO, TBBz, or CX4945 for 3 hours. The antibody against CK2 substrate phosphorylation indicates activity of CK2. Y-tubulin was used as loading control (n=3). (C) Representative immunostaining of epicardial cells which were treated for 5 days with TBBz or CX4945 or epicardial cell medium as control (n=3). (D) Results from LOPAC1280 screen in the three individual screens for TBBz and TBB.

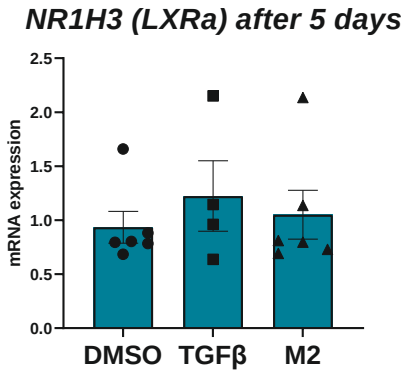

Fig. S3 | M2 may not induce epiMT via LXRα

mRNA expression levels for NR1H3 in epicardial cells that were treated for 5 days with DMSO, TGFβ or M2 (n=3).

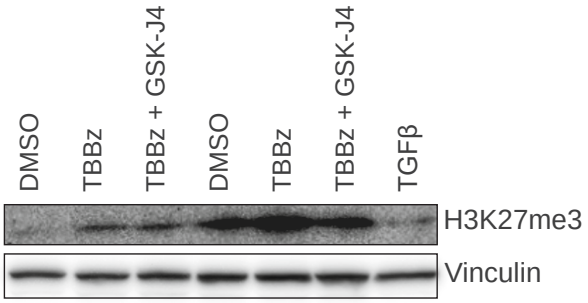

Fig. S4 | Effect of TBBz on H3K27me3 levels. Controls corresponding to Figure 5I. Western blot of protein expression levels for H3K27me3 and loading control Vinculin for epicardial cells treated with DMSO (n=3), TBBz (n=3), TBBz+GSK-J4 (n=2), or TGFβ (n=1) for 3 hours.

Supplementary Table 1 | Selection Screen 1

Screen	Compound ID	SMA (Relative to Control %)	Compound Name	Description
1	431	105,1	2′,3′-dideoxycytidine	Nucleoside analog; reverse transcriptase inhibitor; antiviral
1	1399	76,2	Oltipraz metabolite M2	Oltipraz metabolite M2 acts as a potent inhibitor of LXRa transcriptional activity, and also AMPK activator inducing the phosphorylation of AMPK.
1	917	76,0	8-Methoxymethyl-3-isobutyl-1-methylxanthine	Selective inhibitor of Ca2+-calmodulin-dependent phosphodiesterase (PDE I)
1	777	64,2	LY-367,265	Inhibits serotonin reuptake; 5-HT2A serotonin receptor antagonist
1	15	57,8	PD 0325901	PD 0325901 is a potent MKK1 (MEK1) and MKK2 (MEK2) inhibitor
1	832	57,6	Ivermectin	Positive allosteric modulator of alpha7 neuronal nicotinic acetylcholine receptor; also modulates glutamate-GABA-activated chloride channels
1	152	54,7	Alaproclate hydrochloride	Potent and selective serotonin reuptake inhibitor
1	799	54,0	Ketoconazole	Potent inhibitor of cytochrome P450c17 enzyme; antifungal agent
1	416	53,2	Carvedilol	Antihypertensive; cardioprotective
1	508	51,7	3-deazaadenosine	Antiviral
1	1041	50,3	Nortriptyline hydrochloride	Tricyclic antidepressant
1	779	49,3	CP-154526 hydrochloride	CP-154526 is a selective, non-peptide antagonist of corticotropin releasing factor receptors (CRF1).

Supplementary Table 1 *(Continued)*

Screen	Compound ID	SMA (Relative to Control %)	Compound Name	Description
1	1413	46,8	PD-166866	PD-166866 is a selective inhibitor of the FGF-1 receptor tyrosine kinase (FGFR1) with IC50 = 55 nM, and no effect on c-Src, PDGFR-b, EGFR or insulin receptor tyrosine kinases or MEK, PKC, and CDK4.
1	862	45,3	L-687,384 hydrochloride	Putative sigma-1 receptor agonist
1	796	44,7	L-N6-(1-Iminoethyl)lysine hydrochloride	Selective inducible nitric oxide synthase (iNOS) inhibitor.
1	778	44,2	Leflunomide	Immunosuppressive; its metabolite, a malononitrile derivative, inhibits dihydroorotate dehydrogenase (in the de novo pyrimidine synthesis pathway) and several protein tyrosine kinases
1	773	44,0	m-Iodobenzylguanidine hemisulfate	Antitumor agent which inhibits ADP ribosylation; induces changes in the mitochondrial membrane potential, activation of caspase-3 and DNA fragmentation
1	167	43,9	TBBz	Cell-permeable casein kinase 2 (CK2) inhibitor.
1	958	43,1	Eupatorin	Eupatorin acts as an antiproliferative in cells expressing the CYP1A- family. It induces G2/M block follow by apoptosis in cells expressing the CYP1A- family
1	1070	42,2	Nimodipine	Potent L-type Ca2+ channel antagonist
1	774	42,1	Imetit dihydrobromide	Potent and selective H3 histamine receptor agonist

Supplementary Table 1 *(Continued)*

Screen	Compound ID	SMA (Relative to Control %)	Compound Name	Description
1	795	41,8	Rizatriptan benzoate salt	Rizatriptan is a serotonin 5HT-1B/1D-receptor agonist used to treat migraine
1	557	41,1	Dipyridamole	Coronary vasodilator; adenosine transport inhibitor
1	854	40,9	(±)-Isoproterenol hydrochloride	Sympathomimetic amine acting almost exclusively on beta adrenoceptors; bronchodilator
1	621	40,9	Fluspirilene	Dopamine receptor antagonist; antipsychotic
1	643	40,8	5-Fluorouracil	Thymidylate synthetase inhibitor; leads to accumulation of cells in S phase
1	322	40,4	Caffeic acid phenethyl ester	NFkB inhibitor
1	775	39,7	Agomelatine	Agomelatine is an extremely potent agonist at both melatonin receptors (MT1 and MT2), with additional antagonism at 5HT2C
1	801	38,3	Olvanil	Vanilloid receptor agonist
1	250	38,2	ML-9	Myosin light chain kinase (MLCK) inhibitor

Supplementary Table 2 | Selection Screen 2

Screen	Compound ID	SMA (Relative to Control %)	Compound Name	Description
2	1197	97,7	Phenamil methanesulfonate	Irreversible inhibitor of amiloride-sensitive Na+ channels; derivative of amiloride
2	1399	84,3	Oltipraz metabolite M2	Oltipraz metabolite M2 acts as a potent inhibitor of LXRa transcriptional activity, and also AMPK activator inducing the phosphorylation of AMPK.
2	1514	69,8	Tyrphostin AG 538	Insulin growth factor 1 (IGF-1) receptor protein tyrosine kinase inhibitor
2	1121	58,2	SB 216763	Potent, selective, cell permeable inhibitor of glycogen synthetase kinase-3 (GSK-3).
2	628	52,1	Phenserine	Selective, non-competitive acetylcholinesterase (AChE) inhibitor.
2	1149	50,8	R(-)-N6-(2-Phenylisopropyl) adenosine	A1 Adenosine receptor agonist
2	580	42,8	(-)-Physostigmine	Cholinesterase inhibitor
2	271	42,4	BTCP hydrochloride	Selective blocker of dopamine reuptake
2	1065	38,8	CID 11210285 hydrochloride	CID 11210285 is a cell-permeable, potent and selective activator of Wnt signaling without inhibiting GSK-3ß.
2	885	36,3	6-Methyl-2-(phenylethynyl)pyridine hydrochloride	Highly selective, non-competitive mGluR5 metabotropic glutamate receptor antagonist
2	1156	35,3	PD-184161	PD-184161 is a MEK inhibitor.
2	1222	30,2	SMER28	Small molecule modulator of mammalian autophagy.
2	1533	23,0	CP-135807	CP-135807 is a selective 5-HT1D agonist

Supplementary Table 2 *(Continued)*

Screen	Compound ID	SMA (Relative to Control %)	Compound Name	Description
2	748	22,6	Bendamustine hydrochloride	DNA-alkylator with a distinct pattern of activity. Bendamustine activates DNA-damage stress response and apoptosis; inhibits mitotic checkpoints; and induces mitotic catastrophe.
2	869	22,4	PF-429242 dihydrochloride	PF-429242 is a potent inhibitor of S1P (cellular proprotein convertase sterol regulatory element-binding protein (SREBP) site 1 protease).
2	290	20,1	Icaritin	Enhances osteoblastic differentiation of mesenchymal stem cells (MSCs) while it inhibits adipogenic differentiation of MSCs by inhibiting PPAR-gamma pathway.
2	1002	19,6	Levetiracetam	Anticonvulsant; antiepileptic; exact mechanism of action is unclear but may be related to a synaptic vesicle protein.
2	1111	18,9	LP44	A high affinity 5-HT7 receptor agonist.
2	35	18,8	Atropine methyl bromide	Competitive muscarinic acetylcholine receptor antagonist
2	666	18,6	Fluphenazine dihydrochloride	Dopamine receptor antagonist; antipsychotic
2	1241	17,7	Prochlorperazine dimaleate	Antipsychotic agent; used in the treatment of spastic gastrointestinal disorders
2	1267	17,2	(+)-CP-99994 dihydrochloride	(+)-CP-99994 is a selective neurokinin (NK)-1 tachykinin antagonist.
2	568	14,6	SP600125	Selective c-Jun N-terminal kinase (c-JNK) inhibitor.
2	292	14,2	Carbachol	Acetylcholine receptor agonist

Supplementary Table 2 *(Continued)*

Screen	Compound ID	SMA (Relative to Control %)	Compound Name	Description
2	1250	13,7	Ritodrine hydrochloride	beta2-Adrenoceptor agonist; relaxes uterine muscle contractions
2	1509	12,1	EMPA	EMPA is a potent, selective OX2R antagonist
2	167	12,1	TBBz	Cell-permeable casein kinase 2 (CK2) inhibitor.
2	298	11,4	Chlorpromazine hydrochloride	Dopamine receptor antagonist; anti-emetic; antipsychotic
2	800	11,0	L-701,324	Selective antagonist at the glycine site of the NMDA glutamate receptor
2	650	10,9	RepSox	RepSox Inhibits TGF-beta receptor signaling. Retroviral transduction of Sox2, Oct4, and Klf4 genes results in direct reprogramming of somatic cells into induced pluripotent stem cells (iPSCs).

Supplementary Table 3 | Selection Screen 3

Screen	Compound ID	SMA (Relative to Control %)	Compound Name	Description
3	290	171,9	Icaritin	Enhances osteoblastic differentiation of mesenchymal stem cells (MSCs) while it inhibits adipogenic differentiation of MSCs by inhibiting PPAR-gamma pathway.
3	105	138,3	Acetohexamide	Stimulates insulin release
3	617	135,8	Sunitinib malate	Sunitinib malate is a receptor tyrosine kinase inhibitor, which targets VEGF-R1, VEGF-R2, VEGF-R3, PDGF-Ra, PDGF-Rß, KIT, FLT3, CSF-1R, and RET. Sunitinib malate is an anticancer drug.
3	267	129,2	Bepridil hydrochloride	Non-selective Ca2+ channel blocker which stimulates the binding of 1,4-dihydropyridine-based drugs to Ca2+ channels; anti-anginal
3	430	112,5	(-)-alpha-Methylnorepinephrine	Active enantiomer; adrenoceptor agonist; vasoconstrictor; antihypertensive
3	94	106,4	2-Hydroxysaclofen	GABA-B receptor antagonist
3	460	101,0	Chlormezanone	Anxiolytic; muscle relaxant
3	278	99,1	DL-Buthionine-[S,R]-sulfoximine	Glutathione synthesis inhibitor
3	104	97,1	1-Allyl-3,7-dimethyl-8-p-sulfophenylxanthine	Weak A2 adenosine receptor antagonist; water soluble
3	1121	95,9	SB 216763	Potent, selective, cell permeable inhibitor of glycogen synthetase kinase-3 (GSK-3).
3	740	91,5	L-165,041	Peroxisome proliferator-activated receptor (PPAR) gamma agonist.
3	1172	90,4	BF-170 hydrochloride	Exhibits 3-fold greater binding affinity to tau than amyloid beta fibrils. Does not inhibit amyloid beta.

Supplementary Table 3 *(Continued)*

Screen	Compound ID	SMA (Relative to Control %)	Compound Name	Description
3	1458	63,5	U-74389G maleate	Free radical lipid peroxidation inhibitor
3	1409	57,5	TCPOBOP	Constitutive androstane receptor (CAR) agonist; most potent known member of the phenobarbital-like class of CYP-inducing agents
3	140	53,3	1-Amino-1-cyclohexanecarboxylic acid hydrochloride	Synthetic amino acid that crosses the blood-brain barrier by the Large Neutral Amino Acid carrier system
3	1386	50,7	Tetradecylthioacetic acid	Peroxisome proliferator-activated receptor (PPAR)-alpha agonist
3	987	49,5	H-8 dihydrochloride	Potent inhibitor of cAMP- and cGMP-dependent protein kinase
3	476	48,4	N,N,N′,N′-Tetramethylazodicarboxamide	Thiol-oxidizing agent
3	247	47,5	BMY 7378 dihydrochloride	Partial 5-HT1A serotonin receptor agonist; alpha1D adrenoceptor antagonist
3	1384	46,9	SDZ-205,557 hydrochloride	Potent and selective 5-HT4 serotonin receptor antagonist
3	1240	45,8	Ammonium pyrrolidinedithiocarbamate	Prevents induction of nitric oxide synthase (NOS) by inhibiting translation of NOS mRNA
3	107	43,9	2,3-Butanedione monoxime	Blocks ATP-sensitive K+ channels
3	248	43,8	BRL 54443 maleate	Potent 5-HT1E/1F serotonin receptor agonist
3	1383	43,8	SR-95531	Specific GABA-A receptor antagonist; does not affect GABA-transaminase or glutamate-decarboxylase activities.
3	418	43,7	S(-)-Pindolol	Beta adrenergic receptor antagonist; vasodilator. Non-selective 5-HT1 serotonin receptor ligand.

Supplementary Table 3 *(Continued)*

Screen	Compound ID	SMA (Relative to Control %)	Compound Name	Description
3	944	42,7	Melatonin	Endogenous neurohormone which controls photo-periodic biological rhythms
3	1072	41,8	Oleic Acid	Activates protein kinase C in hepatocytes; uncouples oxidative phosphorylation
3	1181	41,7	Pergolide methanesulfonate	Dopamine receptor agonist; antiparkinsonian
3	269	41,4	Alfuzosin hydrochloride	alpha-adrenergic blocker used to treat benign prostatic hyperplasia (BPH)
3	447	40,4	(±)-CGP-12177A hydrochloride	Mixed beta adrenoceptor agonist/antagonist

Supplementary Table 4 | Selection Overlapping hits

Compound ID	SMA Screen 1 (Relative to Control %)	SMA Screen 2 (Relative to Control %)	SMA Screen 3 (Relative to Control %)	Compound Name	Description
15	57.8	9.9	38.2	PD 0325901	PD 0325901 is a potent MKK1 (MEK1) and MKK2 (MEK2) inhibitor
167	34.5	12.1	59.7	TBBz	Cell-permeable casein kinase 2 (CK2) inhibitor.
290	11.8	20.1	171.9	Icaritin	Enhances osteoblastic differentiation of mesenchymal stem cells (MSCs) while it inhibits adipogenic differentiation of MSCs by inhibiting PPAR-gamma pathway.
446	13.1	10.6	73.2	CP-91149	CP-91149 is a selective glycogen phosphorylase inhibitor.
508	51.7	10.3	16.7	3-deazaadenosine	Antiviral
676	-1.5	10	83.1	MHPG piperazine	Norepinephrine metabolite
869	35.6	17.7	1.9	PF-429242 dihydrochloride	PF-429242 is a potent inhibitor of S1P (cellular proprotein convertase sterol regulatory element-binding protein (SREBP) site 1 protease).
917	76	-2.2	35.8	8-Methoxymethyl-3-isobutyl-1-methylxanthine	Selective inhibitor of Ca2+-calmodulin-dependent phosphodiesterase (PDE I)
1121	19.6	58.2	95.9	SB 216763	Potent, selective, cell permeable inhibitor of glycogen synthetase kinase-3 (GSK-3).

Supplementary Table 4 *(Continued)*

Compound ID	SMA Screen 1 (Relative to Control %)	SMA Screen 2 (Relative to Control %)	SMA Screen 3 (Relative to Control %)	Compound Name	Description
1399	76.2	84.3	8.4	Oltipraz metabolite M2	Oltipraz metabolite M2 acts as a potent inhibitor of LXRa transcriptional activity, and also AMPK activator inducing the phosphorylation of AMPK.